AIMS Materials Science, 5(4): 559–590.
DOI: 10.3934/matersci.2018.4.559
Received: 18 February 2018
Accepted: 19 June 2018
Published: 28 June 2018

http://www.aimspress.com/journal/Materials

Review

Mechanical behaviors and biomedical applications of shape memory materials: A review

Chunsheng Wen[1,†], Xiaojiao Yu[1,†], Wei Zeng[1,2], Shan Zhao[1], Lin Wang[1], Guangchao Wan[1], Shicheng Huang[1], Hannah Grover[1] and Zi Chen[1,*]

[1] Thayer School of Engineering, Dartmouth College, Hanover, NH 03755, USA
[2] Center for Applied Biomechanics, University of Virginia, Charlottesville, VA 22911, USA

* **Correspondence:** Email: Zi.Chen@dartmouth.edu; Tel: +16036466475.

† These two authors contributed equally.

Abstract: A shape memory material (shape memory alloy (SMA) or shape memory polymer (SMP)) can experience large deformation and recover its original shape when exposed to a specific external stimulus. Shape memory materials have drawn significant attention due to their applications in biomedical devices, which typically require appropriate mechanical biocompatibility, including elastic modulus compatibility, adequate strength and fracture toughness, and superior fatigue resistance. In this review, we provide an overview of mechanisms and biomedical applications of some common SMAs and SMPs, experimental evidences on their mechanical biocompatibility, and some key aspects of computational modeling. Challenges and progress in developing new shape memory materials for biomedical applications are also presented.

Keywords: shape memory alloy; shape memory polymer; biomedical application; mechanical biocompatibility; computational modeling

1. Introduction

Shape memory materials are known for their capability of programming their shape changing behaviors [1]. Even after being forced to assume a temporary shape, the deformed configuration can recover its original state under certain external stimulation, such as thermal [2], mechanical [3],

electrical [4], electro-magnetic [5], or chemical [6]. Shape memory materials are ideal candidates for developing reconfigurable structures and biomedical devices because of their good stimuli-responsiveness and various shape changeability [7]. For example, medical implants made of shape memory materials, such as stents and heart valves, can be deformed into relatively small size before they are implanted into the human body during minimally invasive surgery (MIS), while being able to expand and recover to a larger shape when exposed to body temperature [8].

Shape memory alloys (SMAs) and shape memory polymers (SMPs) are the most widely studied shape memory materials [9–12]. The mechanism of SMAs is associated with the diffusionless phase transformation by well-coordinated shear dominant atomic displacement between austenite (the high temperature phase with a face-centered cubic structure) and martensite (the low temperature phase with low crystallographic symmetry and a body-centered tetragonal structure). The shape memory effect (SME) and superelasticity (SE), also called pseudoelasticity (PE) are the two most frequently utilized behaviors for SMAs. Both behaviors can recover the original shape, through heating of the SME and unloading of the SE, respectively. Correspondingly, the reversible martensitic transformation is induced by temperature for SME but by stress for SE [3,13,14]. Generally, SME of SMPs can be achieved by designing various polymers with special molecular structure and different transition segments. The fixity segment determines the permanent shape and switching segment is responsible for temporary shape [15]. Thermal-induced SMPs as the most widely and successfully studied in the field of smart materials, have obtained increasing attention. SMPs are easier to process and can exhibit up to 200% strain, which is much larger compared to 10% strain for SMA [16].

In order to be incorporated into biomedical devices, shape memory materials need to be biocompatible besides meeting physical and electrochemical requirements [17]. For example, the basic requirement for achieving mechanical biocompatibility for an implant is to bear large stress, be mechanically biocompatible for a long period, be functionally stable, and have an appropriate elastic modulus [18]. Otherwise, plastic deformation can occur in the implant and cause failure or functional degradation. There have been a number of excellent reviews on shape memory materials' application in biomedical field [3,19,20]. In comparison, here we particularly focus on the mechanical behaviors of the SMAs and SMPs, particularly on the mechanical biocompatibility.

The goal of this review is to provide an overview of the shape memory mechanism of the most common shape memory materials and address the governing factors that affect their mechanical properties based on the results of experimental and computational modeling, which can aid in the design and fabrication of advanced shape memory materials for biomedical applications. Here, we review the physical mechanisms and biomedical applications of SMAs and SMPs, experimental work on their mechanical biocompatibility, and identify various external and internal factors that influence the mechanical behaviors. Computational modeling works on the kinetics and mechanical behavior of SMAs and SMPs are also introduced. The challenges of designing and fabricating shape memory materials for biomedical applications are further discussed.

2. Mechanism and biomedical applications of shape memory materials

2.1. Shape memory alloys

2.1.1. Mechanism

As one of the most prominent functional metallic materials, SMAs are uniquely characterized by their SME and SE/PE. In SME, a deformed alloy can recover its original shape simply by heating; while in SE, the alloy can be deformed severely and recover its original shape once the load is released. Martensitic transformation, as the common origin of SME and SE in SMAs, is a class of diffusionless phase transformation and is characterized by well-coordinated shear dominant atomic displacement. Martensitic transformation starts from austenite (a high temperature phase or parent phase), which is typically a cubic phase such as a body centered cubic (bcc) or face centered cubic (fcc) structure. The crystal structure is then cooled to below martensitic transformation temperature and transforms into a product phase (martensite phase or martensite) with low crystallographic symmetry. Four important transformation temperatures are used to describe the temperature ranges: Martensite start temperature (M_s), martensite finish temperature (M_f), austenite start temperature (A_s), and austenite finish temperature (A_f) [3,13].

The general mechanism of SME and the corresponding changes in atomic structures model during transformation is illustrated in Figure 1a. In this case, the martensitic transformation temperature of the SMA is sufficiently above the room temperature. The sample can be easily deformed by a mechanical load at a temperature lower than M_f, because the strain is accommodated by the growth of single variant martensite favored by the stress at the expense of others, and the residual deformation remains after unloading. When the deformed sample is heated to a temperature above A_f subsequently, the single variant martensite transforms back to austenite and the original shape recovers. This occurs because all the variants are originally formed from one single austenite crystal. A sample in the martensite phase can be obtained when cooled to room temperature, however, its shape does not change due to the self-accommodated multi-variant martensite structures.

It should be emphasized that only the austenite shape is memorized in the SME described above, and this is referred to as one-way SME (OWSME). In addition, a two-way SMA (TWSMA) can memorize its shape at both high (austenite shape) and low (martensite shape) temperatures. However, TWSMA is less commercially used due to the additional "training" requirement, and it generally produces less recovery strain than what is provided by OWSMA for the same material [21–24]. Meanwhile, TWSME tends to deteriorate quickly especially at high temperatures [13], so the stability and repeatability are far from optimal [25]. Therefore, OWSME is still the most widely used in practice to provide reliable performance [26].

The martensitic transformation involved in SME is induced by temperature (thermally). In addition, it can also be induced by stress (mechanically), associated with the SE [3,13,14]. Tsuchiya (2011) illustrated the mechanism of SE in Figure 1b, which indicate that the SMA is deformed by a mechanical load at a temperature above A_f. When the sample with the fully austenite phase is subjected to a stress, it may deform by stress induced martensitic transformation. Upon unloading, the martensite will completely transform back to austenite because it is not thermodynamically stable at that temperature, so the original shape recovers.

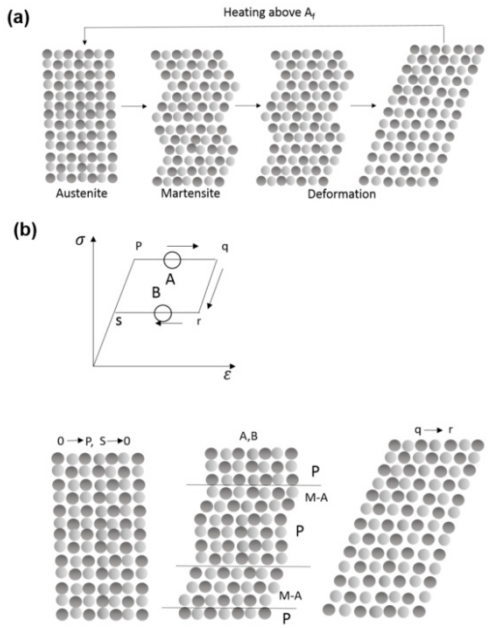

Figure 1. Mechanism of (a) SME and (b) SE. The upper part of the figure shows a typical superelastic stress (σ)-strain (ε) curve. P: Parent phase, M: Martensite phase. The three lower figures schematically illustrate the atomic arrangements in the different states of the sample marked as p, q, r, s, A and B in the stress-strain curve. Reprinted from [14] with permission.

For NiTi alloys, the typically used biomedical SMA, previous research indicated that the precipitation of different second phases would influence the starting temperature of martensitic transformation (M_s) and the type of martensitic transformation (R-phase or B19' martensitic transformation) [27–32]. For B19' transformation, as the content of Ni increases, M_s significantly decreases; for R-phase transformation, the transformation is more likely to occur if there is higher coherency of the Ni_4Ti_3 phase in the parent phase [30–32]. However, with increasing temperature and time, the Ni_4Ti_3 phase would grow and decompose into Ni_3Ti_2 and Ni_3Ti phases. By studying Ni-rich NiTi alloys at different heat treatments, Qin et al. [33] found that the lower the M_s temperature, the higher the hardness became. This can be ascribed to the difficulty in the occurrence of stress-induced B19' martensitic transformation at lower M_s temperature.

Recently, Luo et al. [34] studied the effects of extrusion and re-extrusion on the microstructure evolutions and textures of second phase precipitates in NiTi alloys using the high-resolution electron backscatter diffraction (EBSD). Results indicated that extruding and re-extruding the as-received NiTi shape memory alloy produced a ⟨111⟩texture parallel to ED (extrusion direction) and {110}⟨uvw⟩texture parallel to TD (transverse direction), and a more homogeneous microstructure with a higher hardness. Using EBSD and TEM techniques, Luo et al. [35] also studied that the non-deforming second phase precipitates resulted in inhomogeneous deformation and the sharp increase in dislocation density in the surrounding matrix, leading to the recovery and recrystallization of the surrounding matrix.

2.1.2. Biomedical applications

Because of the unique properties of SMAs, they have attracted a great deal of interest in automotive, aerospace, robotic, and biomedical applications [36]. The three primary types of SMAs used include: NiTi-based, Cu-based, and Fe-based SMAs. Among the three, NiTi-based alloys are most-commonly used because of their excellent SME and SE [3]. Cu-based and Fe-based SMAs, such as CuZnAl, CuAlNi, and FeMnSi, are low-cost and commercially available, but the usage is limited due to their poor thermal cycle properties, low yield stress, so can hardly replace NiTi-based alloys in prime position in the industrial market [37,38].

NiTi-based SMAs are significantly more expensive than other conventional biomedical metal materials, such as stainless steel. However, they exhibit some excellent characteristics as ideal candidates for biomedical applications, such as high corrosion resistance [40], good biocompatibility [41–43], non-ferromagnetism [44], and unique mechanical behaviors close to those of human tissues and bones [45]. After combining NiTi-based SMAs with minimally invasive surgery (MIS), they have made significant breakthroughs and achieved great success in this area. NiTi-based SMAs are used in medical devices for interventional radiology (e.g., guidewires, stents, stents grafts, inferior vena cava filters), surgical devices for endoscopic and laproscopic surgery, and orthopedics [3,45]. Other medical applications include implants [46,47], aneurism patches [48], eyeglass frames [49], and active catheters [50,51]. Some of the typical biomedical applications of NiTi based SMAs (e.g., orthodontic arch wire, guided wire, bone fixation, and stent) are shown in Figure 2. The fatigue and fracture behavior of NiTi based SMAs have been a concern, so their mechanical properties need to be improved to meet the emerging needs of designing smart biomedical devices [45,52–54].

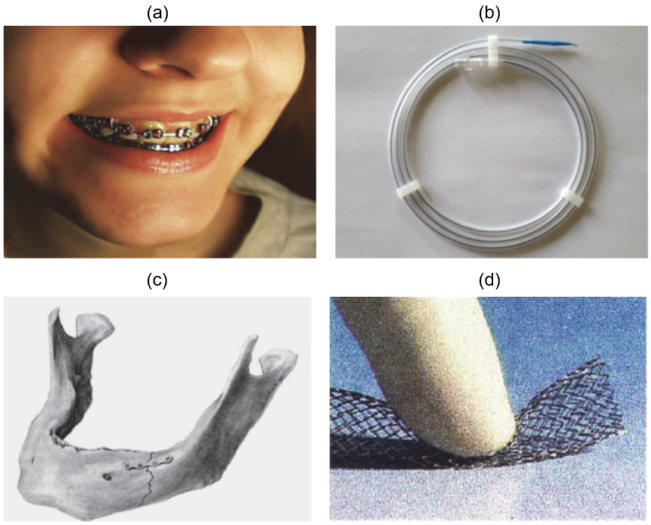

Figure 2. Biomedical applications of NiTi-based SMA. (a) Orthodontic arch wire; (b) Guided wire; (c) Bone fixation; (d) Stent. Reprinted from [39] with permission.

2.2. Shape memory polymers

2.2.1. Progress and mechanism

SMPs represent a class of smart polymeric materials that can be programmed to fix in a deformed state and subsequently recover to the initial state when exposed to an external stimulus [55], such as heat [56–59], moisture [60], pH [61,62], light [63], electricity [64], alternating magnetic field [65], radiation [66] and laser heating [67], microwaves [68,69], pressure [70], solvent or solvent vapors [71], and so forth.

From a mechanism standpoint, SMPs are different from SMAs that are based on the martensitic transformation. SMPs possess special molecular structures that consist of a fixity phase and a reversible phase, as shown in Figure 3, which can describe almost any SMPs system. Here, the fixity phase (net-point) is responsible for the stabilization of the permanent shape, which is formed by chemical or physical crosslinking or supramolecular bonding. Similarly, the reversible phase (switching unit) is responsible for the shape fixity and shape recovery upon different stimuli. The reversible phase contains crystallization, liquid crystallization, light reversible bonding, glass transition or supramolecular hydrogen bonding.

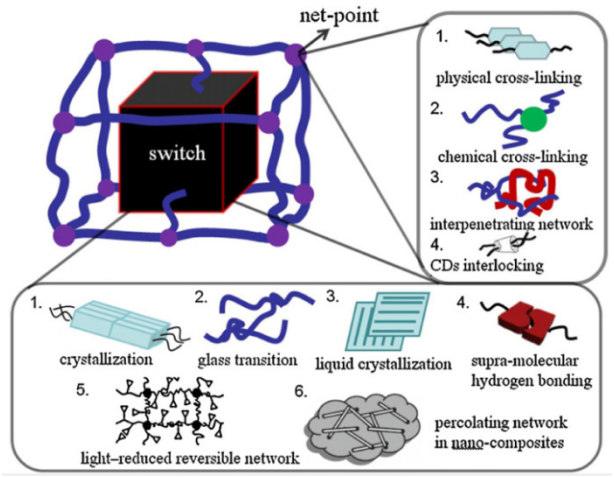

Figure 3. The overall structure of SMPs. Reprinted from [72] with permission.

SMPs typically consist of a net-point and a switching unit. Based on their distinctive nature of net-point, SMPs can be divided into chemical crosslinking or physical crosslinking [73]. Furthermore, per the methods of stimulation, SMPs can be classified into thermal-induced, electric-induced, solvent-induced, or other types which have the ability to recover their shape under related stimuli. Most SMPs can be subdivided into T_g-type and T_m-type SMPs which are activated by T_g (glass transition temperature) and T_m (melting temperature) transition, respectively. Various new shape memory programming methods have emerged, including triple SME [74–76], multi-stimuli [77], multi-functional SMPs [78], two-way SMP [79,80], and temperature memory polymer [81–83].

For T_g-type SMP, the SME is from the reversible soft segment and the stationary hard segment, which correspond to the crystal portion with bridging construction and the amorphous portion, respectively. The amorphous portion exhibits rubber elasticity when heated above T_g and is easy to

be deformed into an arbitrary shape under an external force accompanied by micro-Brownian motion (MBM) of the soft segment. By cooling below T_g followed by unloading, the MBM was frozen, and the distorted shape is largely maintained. Heated again to above its T_g, the reversible frozen segment relaxed, and the hard segment created a recovery force so that the polymer was able to return to the original shape [18].

Compared to SMAs, SMPs have their own advantages, such as lower densities, larger strains, bigger range of tailorable temperatures, easier processing, biocompatibility and biodegradation, and lower cost, which enabled their applications in various areas such as textiles [84], aerospace technologies [85], biomedical applications [86–89], smart actuators [90], etc. Very recently, Zhang et al. [91] designed a radiopaque highly stiff and tough shape memory hydrogel with Young's modulus of 16 MPa and tensile strength of 10 MPa, and the hydrogel strip was successfully transformed into the preprogrammed coil shape in the pigs' renal arteries. This shape memory hydrogel coil showed great promise in renovating traditional metal coils in treating aneurysm.

2.2.2. Biomedical applications

Thermal-induced SMPs have been the most extensively studied due to their promising applications in biomedical devices. SMPs are an attractive candidate in minimally invasive surgeries, smart actuators, drug delivery systems, as well as in special fields, such as orthopedics, photodynamic light therapy, orthodontics, kidney dialysis, and in the therapy of aneurysms or neuroprosthetics [10,26,92–95]. For instance, Lendlein and Langer [96] have prepared a biodegradable thermal-induced SMP used as a suture for tightening and sealing a wound, as shown in Figure 4a. The suture can induce a self-tightening effect under body temperature. Figure 4b shows a drug releasing SMP device that can unfold in a specified location within the body upon the stimulus of body temperature. In addition, the unfolding process will not affect the efficiency of the drug release [97].

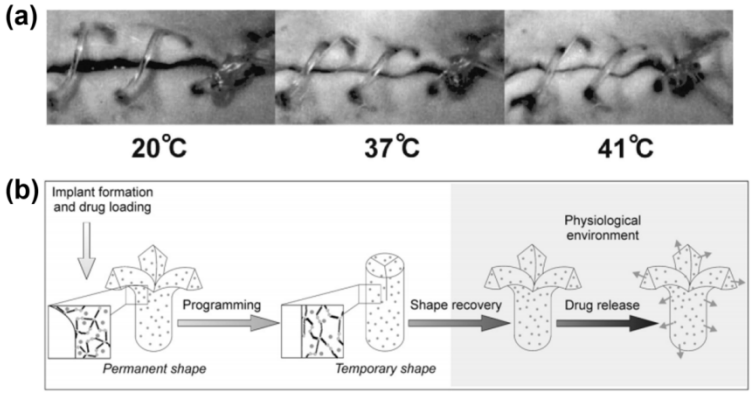

Figure 4. Biomedical application using SMPs. (a) Degradable shape-memory suture for wound closure. Reprinted from [96] with permission; (b) schematic diagram of SMP device with drug releasing function. Reprinted from [97] with permission.

To date, many promising applications ranging from commercial industry to biomedical devices to aerospace engineering have been studied in the field of SMPs. Recent efforts have demonstrated improved capabilities and tunable properties that can eventually be incorporated into medical device

prototypes [98–101]. There are still many challenges that need to be solved such as how to improve stress recovery and cycle time.

3. Experimental studies on mechanical biocompatibility of shape memory materials

The importance of mechanical biocompatibility has been recognized in the development of orthopedics, grafts, and prostheses [102]. To improve the mechanical biocompatibility of shape memory materials, it is necessary to examine their mechanical properties such as elastic modulus, tensile strength, recovery strain, and thermo-mechanical properties before any application.

3.1. Experimental studies on mechanical biocompatibility of SMAs

3.1.1. Elastic modulus

Most biomedical devices are required to have a similar Young's modulus to biological tissues since large differences between the implant's Young's modulus and the surrounding bones can result in the stress-shielding effect (harder implant can remove, or shield stress imposed on the bone and the surrounding tissue, so that the bone materials are reabsorbed without enough stress and their density will deteriorate). This stiffness incompatibility will deteriorate the implant-bone interface and lead to implant failure [18]. To be more specific, the elastic modulus of bone is about 20 GPa [103]. In comparison, solutionized type Ti alloys are reported to have the closest elastic modulus (about 60–80 GPa) among all implanted metallic materials. The elastic modulus of SMAs can be further reduced by changing the material's microstructure through cold working. For example, Niinomi found that the 90% cold worked TNTZ (Ti-Nb-Ta-Zr) possessed a smaller Young's modulus (56 GPa) than a non-worked TNTZ sample (65 GPa) due to texture formation [104]. Thus, the elastic modulus of TNTZ shows anisotropy and can be tuned by growing single crystals in a preferred orientation. For example, the Young's modulus measured at <100> direction E_{100} is only about 35 GPa, comparable to cortical bone as shown in Figure 5.

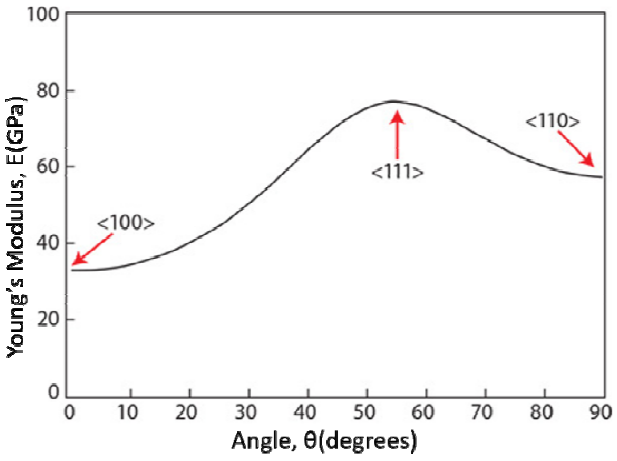

Figure 5. Elastic modulus of a TNTZ single crystal measured in different directions. Reprinted from [105] with permission.

The elastic modulus can also be tuned by introducing porosity into the biomaterial microstructure. For instance, Sadrnezhaad and Hosseini [106] reported that porous NiTi-SMAs prepared by the THP-sintering method had an elastic modulus of 19.8 GPa. The porous NiTi-SMAs also possess a high tensile strength of about 255 MPa, enabling them to bear load as hard-tissue implants. Moreover, as shown in Table 1, Xiong et al. found that both the elastic modulus and plateau stress can be adjusted by varying the porosity of the NiTi alloy foams, where a higher amount of porosity can reduce the Young's modulus and plateau stress [107]. With 30% porosity, the Young's modulus of titanium can be tuned to close to that of a cortical bone [108].

Table 1. Elastic modulus and Plateau stress TiNi alloy foam with different porosities. Reprinted from [107] with permission.

Porosity (%)	Elastic modulus (MPa)	Plateau stress (MPa)
71	860	38.3
80	310	12.1
87	30	1.9

3.1.2. Strength

The strength of a biomaterial also influences the fracture of the implant. If the bone-implant interface fails, a soft tissue could grow at the interface, which will generate a large displacement between the bone and the implant under loading, resulting in severe pain [18]. SMAs such as Ti-Nb-Sn, Ti-Ni and Ti-Nb alloys typically exhibit a double yielding phenomenon in tensile testing as shown in Figure 6. The first yield corresponds to the critical stress required to induce martensite transformation and the reorientation of martensite variants. The second yield point is associated with the critical stress required to induce martensite plastic deformation [109].

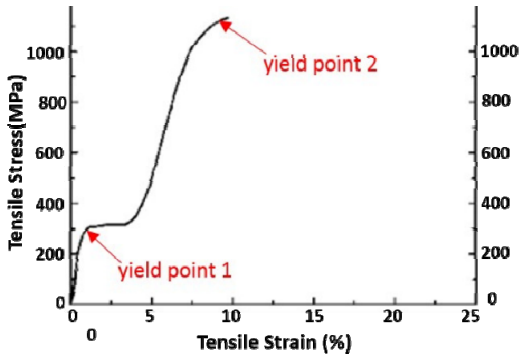

Figure 6. Tensile stress strain curve of the NiTi alloys. Reprinted from [110] with permission.

How to achieve a good combination of appropriate elastic modulus and strength of biomedical materials is an important issue in the design of biomedical devices. The strength of titanium alloys can be increased while keeping the Young's modulus low by cold working after aging, as shown in Figure 7. By varying the material composition, the strength of SMAs can also be tuned. For instance, the yield stress of binary Ti-Nb alloys decreases with the increase of Nb. The yield stress reaches a

minimum when the Nb content is about 26.5%, then increases again as the Nb content increases [111]. The addition of ternary elements such as Ta, Zr, or O were also reported to increase the strength of the SMA [112].

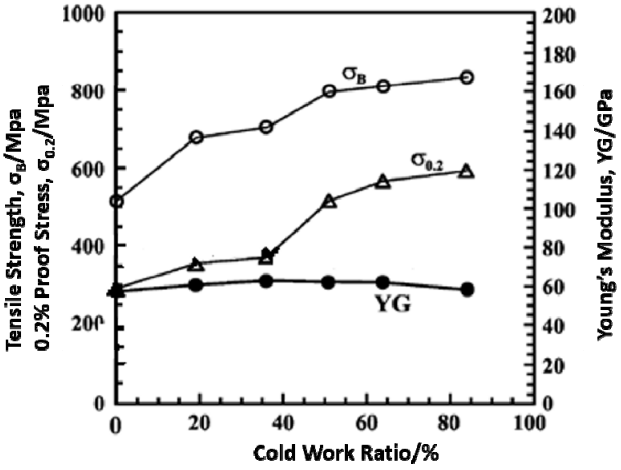

Figure 7. Tensile strength, yield stress, and the Young's modulus of Ti-29Nb-13Ta-4.6-Zr as a function of cold work ratio. Reprinted from [113] with permission.

3.1.3. Fracture toughness

The fracture toughness of SMAs is another important factor to consider when SMAs are applied in biomedical devices. This measures the amount of energy that a material can absorb before it fails. Many brittle materials have high strength but low toughness. For example, many NiTi-based SMAs are prone to fracture. To assess their fracture toughness, macroscopic uniaxial tensile testing and microscopic in situ tensile testing were employed by Chen J, Wang G and Sun W [110] to examine the crack initiation and propagation process. Specimens with different notch acuities were tested. The results showed that the main crack was always initiated at the notch root and propagated in line with the maximum normal stress direction. While the microstructure has a negligible effect on the crack propagation direction, coarser lamellar substructures exhibited worse resistance to crack propagation.

The fracture behavior of superelastic Nitinol alloys was also studied under cyclic loading conditions. Mckelvey and Ritchie [114] examined the cyclic tensile fatigue-crack growth behavior in Nitinol as a function of temperature, microstructure (stable austenite, superelastic austenite, martensite), and load ratio on an electro-servo-hydraulic testing machine. The crack propagation rate was measured at a constant load ratio and the fatigue behavior of the various microstructures was plotted in Figure 8. The fatigue-crack growth resistance of the martensite was found to be superior to that of the stable austenite. The lowest resistance was seen in the superelastic austenite. Moreover, as temperature decreased, the threshold stress intensity increased while the growth rates decreased. For example, the κ_{th} thresholds for martensite were increased from about 3 MPa$\sqrt{m}$ at −65 °C to 5 MPa$\sqrt{m}$ at −196 °C.

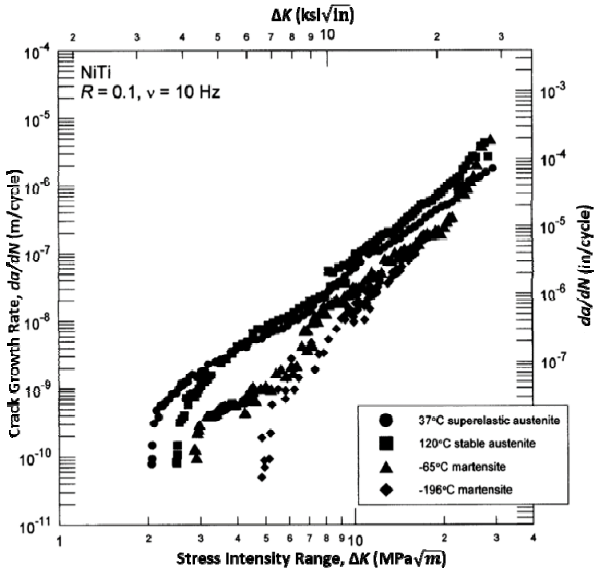

Figure 8. Comparison of the fatigue-crack growth behavior in Nitinol as a function of temperature, in stable austenite (120 ^{o}C). Superelastic austenite (37 ^{o}C), and martensite (−65 ^{o}C and −196 ^{o}C). Reprinted from [114] with permission.

The cyclic fracture behavior of superelasticity of nitinol was further studied by Robertson S, Mehta A, Pelton A, et al. [115] by examining the in situ fatigue crack growth at the micro-scale. Pre-cracked specimens were loaded on the beamline with a custom-designed *in situ* micro tensile loading device to a stress intensity factor (SIF) of (7.5–15 MPa$\sqrt{m}$) with a loading ratio R of 0.5. Fatigue loads were then applied in a displacement-control manner and the local strain at the crack tip was measured with *in situ* high-resolution imaging via X-ray micro-diffraction. This technique can directly examine dynamic phase transformation at a growing crack tip. The local equivalent strain was mapped from the fatigue unloading cycles, which showed the evolution of the transformation zone in Figure 9. The strains in the austenite grains surrounding the crack tip were in the 0.5–1.0% range (green), and the martensite grains were shown as black-colored regions. It is noticeable that the microstructures in the wake of a growing crack transform back to the austenite phase when the stress decreases. They also found that the grain orientation of the surrounding austenite influences the transformation zone, local anisotropic orientation affects the direction of the fatigue crack growth.

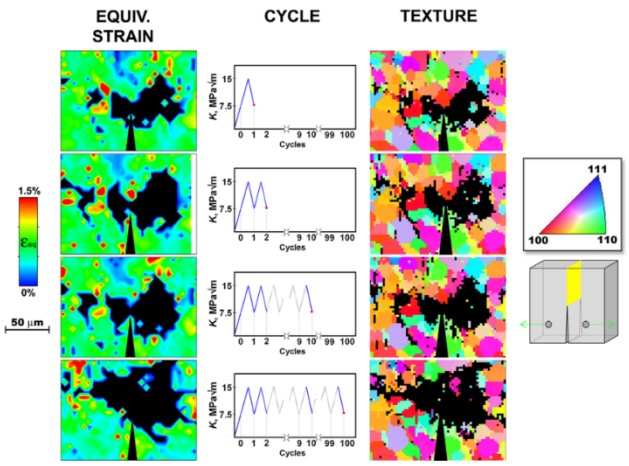

Figure 9. Local equivalent strain maps and grain orientation (texture) maps from fatigue unloading cycles 1, 2, 10 and 100 showing the evolution of the transformation zone. Reprinted from [115] with permission.

3.1.4. Fatigue property

In biomedical devices subjected to cyclic stress, fatigue is often the primary failure mechanism. The implants in peripheral arteries, for instance, can undergo fatigue due to the cyclic loads from the human cardiac rhythm. Cyclic loads can also come from the differences in systolic and diastolic blood pressures. Cumulated fatigue damage can eventually lead to device failure and life threatening scenarios. "Functional fatigue", such as the loss of shape memory or superelasticity effect, can also occur over a number of cycles. The Food and Drug Administration in the United States (FDA) require an intravascular stent to undergo at least 400 million cycles (~10 years) before failure [116]. Hence, how these materials behave under cyclic stress is important to understand. Both classical structural failure and functional fatigue leading to the degradation of shape memory are reviewed in this subsection.

Fatigue properties of materials are often studied with strain-controlled (low cycle fatigue behavior) and stress-controlled (high cycle fatigue behavior) cyclic tests. Fatigue properties are often characterized by the fatigue life (N), resistance to ratcheting strain, fatigue limit, and stress strain hysteresis loops [117,118]. A typical S-N (stress vs. fatigue life) curve can be seen in Figure 10; as the stress amplitude decreases, the fatigue life increases. Thermal mechanical cycling deformation of SMAs were also studied as they often undergo such deformation mode. Recently, a few researchers performed thermal mechanical fatigue test on NiTi by imposing different amplitudes of temperature cycles together with applied stress or strain [119,120]. It was shown that fatigue life of NiTi under thermal mechanical cycling depends on the applied stress/strain and temperature amplitude. It also shows that Martensite transformation becomes more difficult with thermal cycling; the transformation starting temperature decrease with the number of cycles.

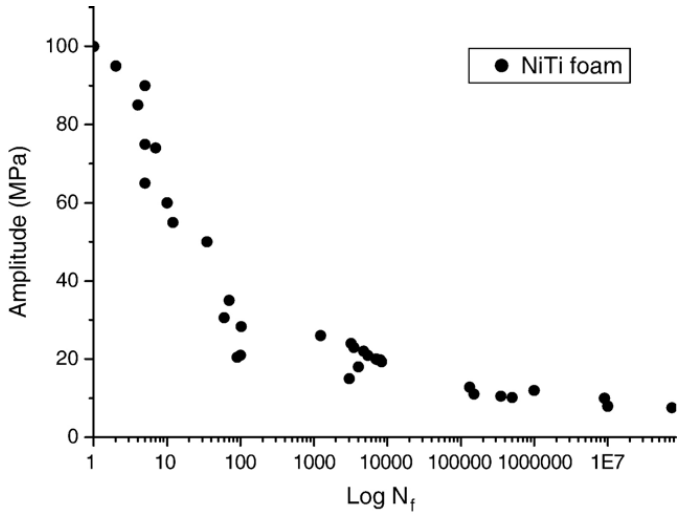

Figure 10. NiTi S-N compression fatigue curve. Reprinted from [121] with permission.

From a microstructural evolution point of view, the fatigue occurs because of the accumulated plastic strains. The accumulated plastic strain typically becomes higher when the stress range increases as shown in Figure 11 (Nayan N, Roy D, Buravalla V, et al. [122]). With the accumulation of plastic strain, the stress required to induce martensitic transformation also decreases. Recently, Kang and Song [123] studied the cyclic tension compression fatigue behavior of superelastic NiTi SMA with constant stress amplitude. They found that the width of the stress-strain hysteresis loop decreases with an increase in the number of cycles, as shown in Figure 12. Because the residual martensite acts as obstacles to the movement of phase transformation front, the stress strain hysteresis loop narrows with the increase in the number of cycles.

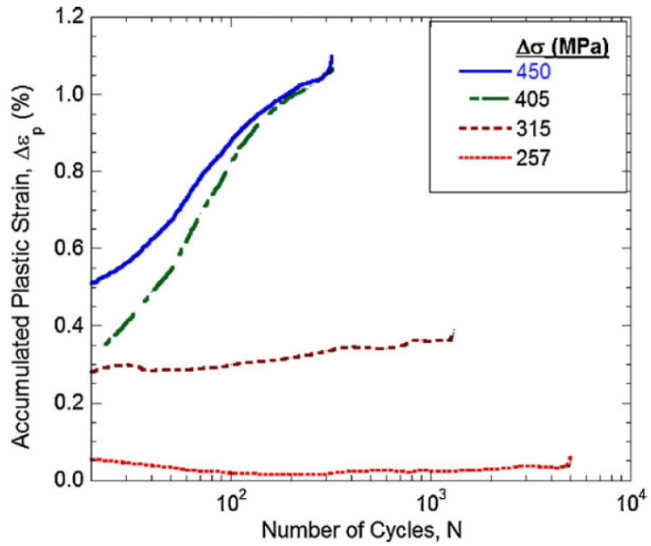

Figure 11. Accumulated plastic strain with number of cycles at different level of stress amplitudes. Reprinted from [122] with permission.

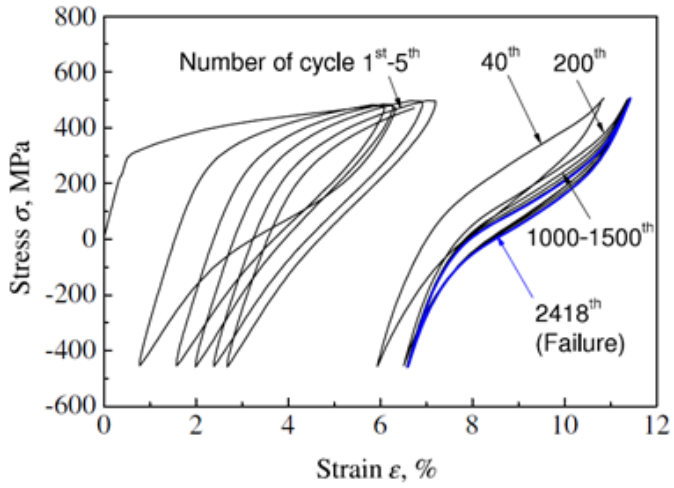

Figure 12. Cyclic tension compression stress-strain curves of superelastic NiTi alloy. Reprinted from [123] with permission.

Not only do those external factors affect the fatigue behaviors, but the internal factors such as the microstructure and composition can play important roles. For instance, the initial microstructure of materials was reported to affect fatigue life under strain-controlled cycling for porous NiTi SMAs. Pore morphology such as shape, size, and distribution can all affect the shape memory effect. The decay of superelasticity in the porous NiTi SMA occurs at a relatively lower cyclic strain level compared with the dense NiTi SMA [124]. Fatigue life was also shown to decrease with the increase of Ni-content in binary NiTi alloys [119]. Ternary NiTi-X alloys have been studied to improve the fatigue resistance and decrease the decay of superelasticity in the binary NiTi alloys. The addition of copper, for example, improves the fatigue resistance during the loading and unloading cycles at a high temperature for better medical applications.

From the studies reviewed above, it is seen that both internal material factors and external loading factors affect SMAs' mechanical properties. Microstructures such as grain size, porosity, texture affect elastic modulus, strength, fracture toughness, and fatigue resistance. Martensite/austenite phase compositions are another influencing internal factor as martensite was reported to have superior fracture and fatigue resistance compared to austenite [20]. Addition of other chemical elements such as Ta, Zr, O and the composition of them also affect mechanical properties. External factors such as cold working, heat treatment, temperature, cyclic stress intensity factor, stress/strain amplitude, mean stress/strain, stress ratio can all influence a SMA's fracture and fatigue resistance.

3.2. Experimental studies on mechanical biocompatibility of SMPs

SMPs possess some superior properties compared with SMAs, such as better flexibility, higher shape recovery ratio, easier fabrication, and better biocompatibility. Hence they can be used as vascular stents, sutures in microsurgery, ocular implants, etc. [73]. The shape memory properties and mechanical properties of SMPs have been widely investigated in recent years. For instance, Fulcher J, Lu Y, Tandon G, et al. [125] investigated the shape memory behavior of epoxy-based thermosetting shape memory resin with a microheater equipped nanoindenter, as shown in Figure 13. Firstly, shape

memory resin is activated at a deformation temperature, above the material's T_g. Then, the resin is cooled to the storage temperature below T_g. Finally, the resin is heated again to a temperature that allows for shape recovery. Schmidt C, Sarwaruddin Chowdhury AM, Neuking K, et al. [126] found that lower recovery ratios occurred in a thermoplastic SMP (Tecoflext) after higher numbers of thermomechanical cycles. Di Prima M, Gall A, Mcdowell D, et al. [127] studied the thermo-mechanical storage and recovery behavior of thermoset shape memory foams under cyclic compression test. They found the existence of a threshold of strain to induce damages under cyclic compression testing and the threshold strain can vary by changing the holding time between compression cycles.

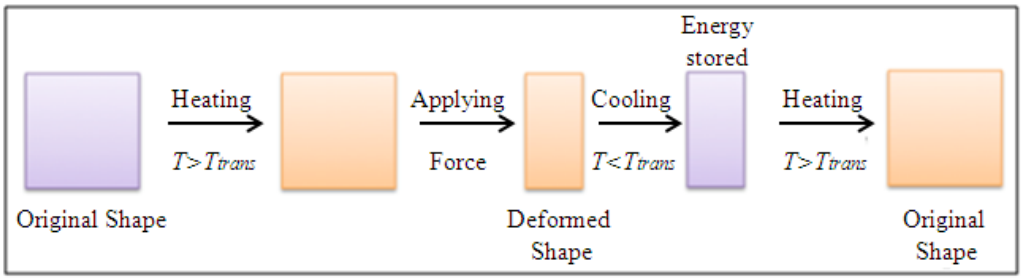

Figure 13. Thermomechanical testing of shape memory polymers. Reprinted from [125] with permission.

However, SMPs generally have lower modulus, strength, and recovery stress, which limit their applications in practice. By changing their molecular weight, phase compositions, cross-linking density, and adding fillers into the polymer network, mechanical properties can be improved. However, shape recovery transition temperature and response might also be affected.

3.2.1. Molecular weight and functional groups

Molecular weight and functional groups of the materials that form SMPs were reported to affect mechanical properties of SMPs. Ahmad M, Xu B, Purnawali H, et al. [128] found that shape memory polyurethane (SMPU) with poly (ε-caprolactone) (PCL) as the soft segment have a higher mechanical strength at room temperature than those of the SMPU with poly (ethylene glycol) as the soft segment, because the former has short molecular chains, higher cross-link density, and lower crystallinity.

Kang et al. (2012) [129] synthesized SMPU foams containing polypropylene glycol (PPG) with different molecular weights (Mw) and functionalities (f). It was found molecular weight is positive correlated with the shape recovery. Lower molecular weight polyol resulted in higher glassy state modulus and high shape fixity due to smaller cell size, higher foam density, strength and glass modulus. Higher molecular weight of polyol resulted in the higher rubbery modulus and better shape recovery due to the higher crosslink density of large molecular weight.

3.2.2. Phase composition

The phase composition has also been found to affect the shape memory effect. Zhang et al. (2009) [130] proposed an immiscible blend SMP system consisted of Styrene-Butadiene-Styrene copolymer (SBS) and PCL composite. Results indicated that an ideal SMP system can be achieved with elastomer

(SBS) being the major continuous phase and switch polymer (PCL) being the minor continuous phase. In this way, the elastic matrix provides the good stretching and recovery performance, while the continuous switch polymer phase affords the good fixing and unfixing performance.

3.2.3. Fiber-reinforced SMP

Guo et al. (2015) [131] found that the shape recovery ratio decreased with an increase in carbon fiber weight fraction. This is due to the formation of composite structures of carbon fibers reinforced SMP matrix. The resilience of composites was larger than that of SMP matrix, therefore, the composites needed a stronger constrained force on their segments and required more energy or more time to accomplish the shape recovery.

3.2.4. Carbon nanotube (CNT)-reinforced SMP

Ni et al. [132] indicated that the reinforcement of a thermoset based SMP from CNT. The reinforcement depended on the extent of CNT which stored the strain energy in the programming procedure, followed by a recovery process where the strain energy would be released. Studies indicated with increasing the weight fraction of vapor growth carbon fibers (VGCF), both the storage elastic modulus and shape memory effect would be dramatically improved.

3.2.5. Iron and ferrite-induced SMP

Mohr et al. [133] incorporated magnetite nanoparticles (iron(III)oxide) in thermoplastic shape-memory biodegradable multiblock copolymer (PDC) and polyetherurethane (TFX), and in this way, the shape recovery was induced magnetically when the programmed samples were exposed to an alternating magnetic field. This noncontact triggering of shape recovery is important for polymers that cannot be warmed up by heat transfer using a heat medium. Results indicated that the shape recovery from magnetic triggering was comparable to that obtained from thermally induced ones; and the amorphous switching phase in nanoparticles of TFX improved the elastic properties even at increased temperature.

3.2.6. Nano-filler (alumina, silica and clay) reinforced SMP

Xu et al. (2010) [134] studied the reinforcing effects from different nanofiller (alumina, silica and clay) on the mechanical behavior of the polystyrene-based shape memory nanocomposites. They found that 1 wt % of nanofillers with rod-like structures (such as clay composites) had the highest storage modulus and energy absorption capacity than spherical nanofillers (such as alumina, silica). This increased reinforcement for rod-like fillers was related to the increased load transfer from the high aspect ratio and specific geometry of the dispersed rod-like fillers to the matrix. For the spherical nanofillers, the composite modulus was more depended on the intrinsic characterizations of nanofillers. For example, the modulus and density of alumina is much larger than that of silica, therefore the enhancement effect for the alumina/PS is more significant than silica.

3.2.7. Nano-filler (hydroxyapatite) reinforced SMP

In addition, Zheng et al. (2006) [135] tested that at the compositional ratio of 1.0–4.0, the shape recovery ratios of PDLLA (Poly(D,L-lactide)) can be improved from 80.6% to 95% with additions of HA (Hydroxyapatite); and the peak shape recovery ratio occurred at 2.0–2.5. This is because in this range, the stationary phase HA particles could best prevent the irreversible strain (ε3), given by the deformation of amorphous PDLLA polymer. If there are too many HA particles, the movements of chain segments of amorphous PDLLA polymer would be greatly restricted during shape recovery. As for thickness-shape recovery relations, Zhang et al. proved that the thicker composites required more recovery time as they needed more energy to get rid of molecular interactions.

3.2.8. Nano-filler (chitosan) reinforced SMP

Wei et al. (2015) [136] studied shape-memory behaviors of electrospun CS (chitosan)/PEO (poly(ethylene oxide)) composite nanofibrous membranes. The authors found that increasing of PEO would provide superior shape-recovery properties. This is because the more active molecule segments would lead to material with better deformability and recovery capacity.

In short, the mechanical property of SMPs is governed by internal factors such as molecular weight and functional group of the materials and cross-linking density of the polymers. SMP-based composites can show different mechanical properties with the incorporation of various filler and phase compositions. Similarly, external factors such as stress/strain conditions and temperatures also influence their mechanical response. Therefore, understanding the intricate relationships between its various controlling factors is the key to design and choose appropriate SMPs to later for specific biomedical applications.

4. Computational modeling on kinetics mechanism and mechanical behavior of shape memory materials

Because of the attractive features of shape memory materials and important applications in biomedical fields, considerable efforts have been made in developing mathematical models on the kinetics mechanism and mechanical behaviors. The deformation behavior of shape memory materials is inherently nonlinear, which requires the development of appropriate constitutive models to characterize the material response. The macroscopic behavior can be predicted by numerical approaches, including finite element methods [137], finite difference methods [36,138,139], molecular dynamics simulations (MDS) [140,141], and phase field modeling [142] (Zhong and Zhu, 2014). For example, the mechanical behavior of SMAs can be driven by a complex stress-induced or thermomechanical solid phase transition, which can be described by some macroscale models. Computational models can also serve as an effective tool for investigating the physical mechanisms underlying the shape-memory response of SMPs and for design optimizations of shape-memory performance under a specific environmental stimulus [143].

4.1. Modeling SMAs

With the broad applications of SMAs in aerospace and medical industries, more interest has been brought up on predicting their responses to certain thermomechanical loadings and many theories have been developed to tackle these challenges. Mechanical analyses on SMA-based devices are often simulated with macroscale models that neglect microscopic details, called phenomenological models. They choose several internal and external variables to describe macroscopic features of SMAs based on continuum thermodynamics [144]. These models can be incorporated into existing numerical methods such as the finite element method. Here, we focus on a series of phenomenological models describing SMAs' properties. The development of macroscale models typically follows a standard procedure: The first step is to select a set of internal variables as macroscopic consequences of the micro-structural changes; the second step is to derive the evolution equations (or flow rules) of these internal variables, which are related to the microscopic transformation mechanisms and should be treated with careful physical considerations; the last step is to carry out numerical simulations to provide some testable predictions, and when possible, compare them with experiments. The modeling of more complex behaviors of SMAs beyond SME and PE (so-called "secondary effects") can be found in a recent review by Cisse, Zaki and Zineb [137].

4.1.1. Macroscale models with no internal variables

Although the selection of internal variables is essential to model construction, there are models which neglect internal variables and only take external variables such as macro-strain or temperature into consideration. A classic example is the polynomial model proposed by Falk [145]. It adopts the expression of the free energy of SMAs in the form of a sixth-order polynomial equation, which involves only two variables, i.e., strain (ε) and temperature (T). The minimal or maximal points of the free energy represent stability or instability of each phase of the SMAs. At a high temperature, the free energy only has one minimal point when the strain equals to zero, denoting the stable austenite phase. At a low temperature, the polynomial has two minimal points with non-zero strains, which means two detwinned martensite phases (stress-induced martensite) exist. At an intermediate temperature, it has three minimal points which represent the stable austenite and two detwinned martensite variants (Figure 14). The polynomial is shown in Eq 1.

$$W(\varepsilon,T)=\frac{a}{2}(T-T_M)\varepsilon^2-\frac{b}{4}\varepsilon^4+\frac{b^2}{24a(T_a-T_M)}\varepsilon^6 \tag{1}$$

Where a and b are material constants which are positive. Austenite is stable above T_a and martensite is stable below T_M. The constitutive equation is then written as Eq 2.

$$\sigma=\frac{\partial W}{\partial \varepsilon}=a(T-T_M)\varepsilon-b\varepsilon^3+\frac{b^2}{4a(T_A-T_M)}\varepsilon^5 \tag{2}$$

The advantage of Falk's model lies within its simplicity and it can also quantitatively reproduce the pseudoelasticity. However, the twinned martensite phase (temperature-induced martensite) is not considered in this model, which suggests that no stable phase exists for $T < T_M$ in a stress-free state.

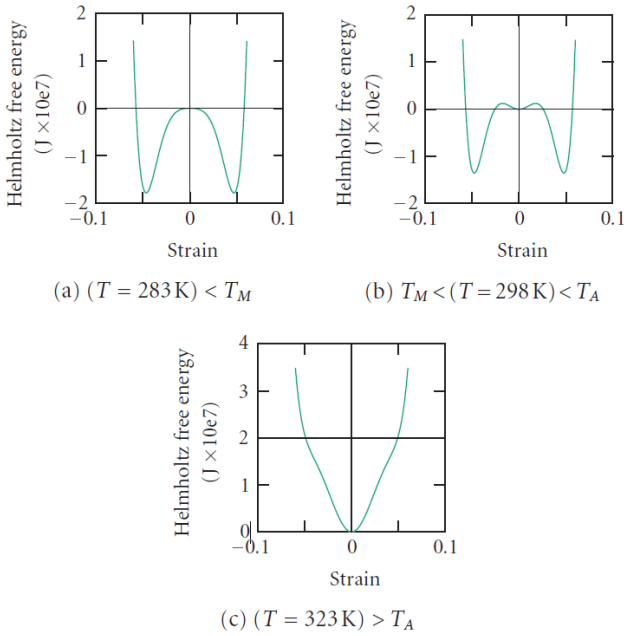

Figure 14. Free energy at different temperatures in Falk's model. Reprinted from [146] with permission.

4.1.2. Macroscale models with phase transformation kinetics

If appropriate internal variables are introduced, the macroscale model can be more robust. It is natural to consider phase transformation kinetics and introduce the martensitic volumetric fraction as internal variables since the martensitic transition is mainly responsible for SME and PE. As the martensitic transformation is non-diffusive in nature, the volumetric fraction of martensite phase can be written as a function of the stress and temperature [146]. Tanaka and Nagaki [147] proposed an exponential function which was shown to be a proper model. For the forward transformation (austenite transforming into martensite), the following function is chosen:

$$\beta = 1 - \exp\left[-a_M\left(M_s - T\right) - b_M\sigma\right] + \beta_0 \tag{3}$$

For the reverse transformation (martensite to austenite), it is replaced by:

$$\beta = \beta_0 \exp\left[-a_A\left(T - A_s\right) - b_A\sigma\right] \tag{4}$$

Where a_M, b_M, a_A and b_A are positive parameters of material properties. M_s denotes the start temperature of martensite formation and A_s is the start temperature of austenite formation.

Later, Liang and Rogers [148] used cosine functions instead of exponential functions to describe the evolution laws. The predictions agreed well with experimental data when this model was applied to study acoustic vibration controls. Another approach has been presented by Brinson [149], in which the martensitic volumetric fraction was split into two parts: Temperature-induced martensite and stress-induced martensite. By categorization of different martensite variants during the transformation process, it became possible to investigate the evolution of twinned martensite, which

went beyond the scopes of other models mentioned above. Numerical simulations for these models were conducted and the results are shown in Figure 15. All these models can reproduce pseudoelasticity. However, this type of models has obvious drawbacks. For example, they all assumed a fixed critical stress for the forward or reverse transformation, in contrast with experiments showing that the critical stress can be altered under cyclic loadings.

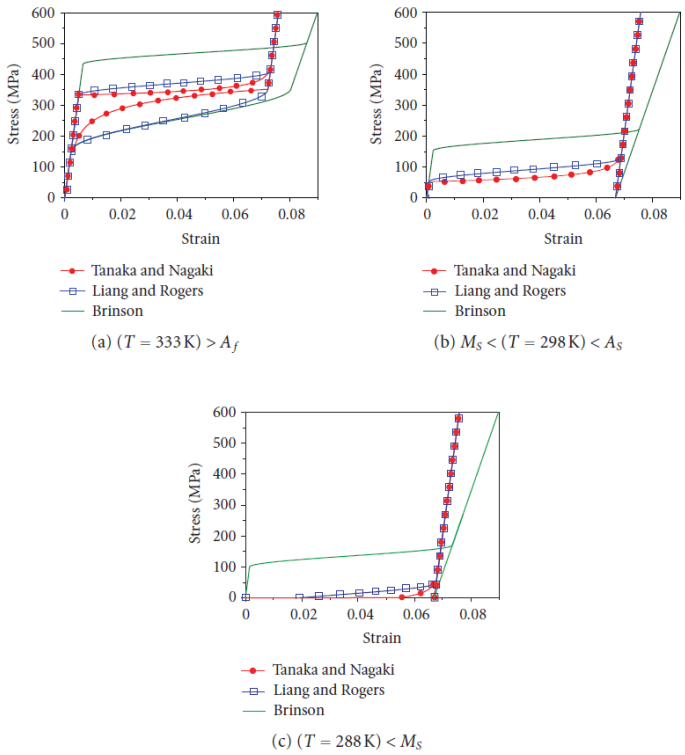

Figure 15. Stress-strain curves for models with assumed transformation kinetics. Reprinted from [146] with permission.

4.1.3. Macroscale models with internal constraints

The evolution equations of internal variables from the models above seemed to be mathematically suitable although no specific physical background was attached. Another class of models derived the evolution equations based on thermodynamics by applying Clausius-Duhem inequality to obtain constraints for internal variables. Panico and Brinson [150] created a three-dimensional (3D) phenomenological model for SMAs to account for the martensite reorientation process under multiaxial loading and non-proportional loading histories. They introduced a tensorial internal variable which represents the inelastic strain in the stress-induced phase transformation process and is divided into two parts, parent phase transformation and martensite variant reorientation, each governed by its own evolution law. The second law of thermodynamic is used to derive the evolution equations of internal variables. Numerical results show that this model can capture several main features of SMAs such as pseudoelasticity or coupling of the axial and the shear inelastic responses under uniaxial or multiaxial tests (Figure 16). Drawbacks of this model, however, lies in the fact that it could not reproduce the asymmetry process in uniaxial tension and compression [151]. Moreover, irreversible plastic strain was not taken into consideration.

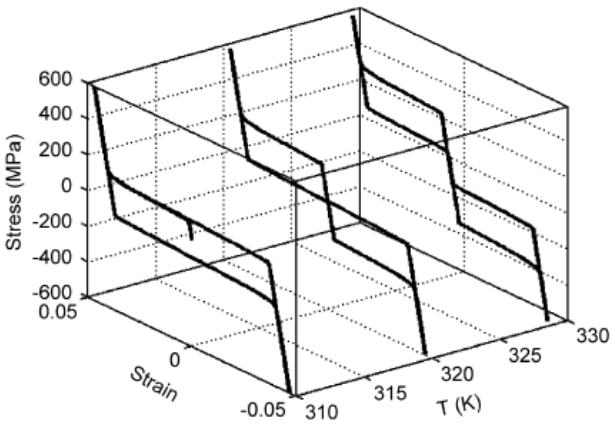

Figure 16. Stress-strain curves under tension-compression uniaxial loading at constant temperature. Reprinted from [150] with permission.

Inspired by Panico's work, Arghavani J, Auricchio F, Naghdabadi R, et al. [152] proposed a 3D phenomenological constitutive model for SMAs by choosing two decoupled internal variables: A scalar variable denoting the amount of stress-induced martensite and a tensorial internal variable representing the average orientation of different variants. Compared to models with only one tensorial internal variable, this decoupling approach gave more freedom to the model and made it possible to characterize the martensite variant reorientation process and its effect on the pure phase transformation in a non-proportional loading process. Flow laws for these two internal variables are obtained by considering Clausius-Duhen inequality in thermodynamics. Further, they developed a time-discrete framework with a backward-Euler integration scheme for numerical implementation. Moumni Z, Zaki W and Maitournam H [153] also proposed a macroscopic model to describe the responses of SMAs under cyclic loadings based on experimental observations. In this model, three state variables are used to represent the residual strain induced by cyclic loading, the internal stress induced by repeated phase changes, and the cumulated martensite volume fraction, respectively. The dissipated energy of the stabilized cycle is simulated and used as a relevant parameter for predicting the number of fatigue life of the materials, which is like the low-cycle fatigue criterion in usual elastoplastic materials. Although they proposed a 3D model for multiaxial loading, their model was only validated in uniaxial loading. Hence, further investigation will be needed for practical applications in 3D shape memory materials.

4.2. Key aspects on modeling SMPs

The shape memory behavior of SMPs involves a variety of shape storage and triggering mechanisms, but for a given environmental stimulus they may share some common mechanisms. For example, amorphous SMPs under thermally induced or photo-induced deformation will experience the glass transition, the crystallization and melt transition mechanism and/or photo-induced network rearrangements [143]. The constitutive models for thermal-sensitive shape memory polymers were comprehensively reviewed by Zhang and Yang [154].

Recently, there has been a growing interest in developing theoretical and numerical frameworks for shape memory behavior of SMPs under large deformation, as well as the computational

simulations for biomedical devices [155]. The thermomechanics model developed by [156] can capture the nonlinear response from the entropic-driven chain rearrangement at high temperatures to study micromechanics and physics underlying the glass transition. Diani J, Liu Y and Gall K [157] then developed a 3D thermoviscoelastic model to simulate the stress-strain-temperature evolution of SMPs in a thermomechanical loading cycle. Furthermore, Li and Xu [158] proposed a thermoviscoelastic model based on the finite deformation theory to examine the shape memory behavior of a thermoset SMP made through cold-compression programming. The model included both structural evolution and pseudo-plasticity, so it was capable of simulating the shape memory effect in this SMP processed by cold compression.

Specifically, the deformation gradient in the model is expressed as the product of a mechanical deformation gradient and a thermal deformation gradient, i.e., $F = F_M F_T$. The thermal deformation gradient is determined using a fictive temperature T_f.

$$F_T = J_T^{1/3}\boldsymbol{I} \tag{5}$$

$$J_T = 1 + \alpha_r\left(T_f - T_0\right) + \alpha_g(T - T_f) \tag{6}$$

Where α_r and α_g represent the thermal expansion coefficient of material in the rubber state and glassy state, respectively.

The mechanical behavior is represented by decomposing the stress into a time-dependent component which refers to the viscoplastic behavior F_v and a time independent component F_e related to rubber-like behavior.

$$F_M = F_e F_v \tag{7}$$

This model is able to capture the characteristics of polymer behaviors including yielding, strain softening, and hardening.

To improve the mechanical properties of SMPs such as the strength and stiffness, hard particles are embedded in the matrices of shape memory polymers. Baghani M, Naghdabadi R, Arghavani J, et al. [159] proposed a phenomenologically constitutive model for thermoset SMPs, in which hard particles are dispersed to strengthen the matrix and modeled using the rule of mixture. The model incorporated three tensorial internal variables to account for the three phases, the rubbery, glassy, and hard phases, during the time evolution of microstructures. By small strains, the strain in this model is decomposed into six components including the strain in hard particles, rubbery phase of polymers, in glassy phase of polymers, thermal strain, irreversible strain, and storage strain.

5. Challenges in designing and fabricating shape memory materials for biomedical applications

Mechanical biocompatibility is an important issue for biomedical applications of SMAs and SMPs, and some challenges in designing and fabricating the shape memory materials remain to be tackled. As the most important kind of SMAs, NiTi-based SMAs show excellent SME, SE, and special biocompatibility; and thus have been widely used in biomedical devices. However, NiTi-based SMAs still have several unfavorable clinical shortcomings that prevent them from being an ideal material for stent devices. One concern with NiTi-based SMAs is related to the release of

nickel ions into body tissues and fluids which can induce toxic and allergic responses [160]. Also, thrombotic complications frequently occur when NiTi-based SMAs are used for vascular implants in small arteries [161]. Therefore, it is necessary to improve the biocompatibility, wear resistance, and corrosion resistance of NiTi-based SMAs. To this end, various surface treatment methods have been developed, each with its own merits and limitations [162–168]. Biodegradability and sterilization are other concerns when designing SMP-based medical devices [101].

The mechanical properties of shape memory materials are influenced by many factors. Grain size and chain length of polymers affects the strength and toughness of materials. Fine grain size leads to high strength and better crack resistance. Long chain polymers tend to decrease chain mobility and result in higher strength and toughness. Heat treatment can refine grains and relieve internal stress due to the cold and hot working of metals. Curation time, cross-link density, and external temperature also affect materials' mechanical properties. Higher temperatures tend to decrease elastic modulus, strength, and fracture toughness. Different types of mechanical properties can be correlated: A high strength often comes with high elastic modulus and fracture toughness can be negatively correlated with strength. A balance of these properties is needed, and so a material's design reduces to a constrained optimization problem. To identify these factors and understand the weight of each factor and their correlations can be challenging. Extensive experimental work and carefully designed computational models are needed.

Even if materials are designed, whether they can be fabricated is another question. The composition of nickel and titanium is critical in defining the transformation temperature of Nitinol alloys. One weight percent of Ni deviation can cause a 100 ^{o}C change in its transformation temperature. Tight chemistry control is required in nitinol alloy fabrication, which poses a significant challenge during the melting process. Nitinol product fabrication, especially complex nitinol parts, is even more challenging because of its high work-hardening rate and high titanium content. The alloys' shape recovery capability makes the formation step difficult at ambient temperatures. Recently, additive manufacturing has been used in the fabrication of NiTi parts. Walker J, Andani MT, Haberland C, et al. [169] produced nitinol parts directly from CAD models by selective laser melting of pre-alloyed powder. Complicated design in the microstructure such as porosity, designed holes, and other intricate features can be realized. Additive manufacturing has also been used in the fabrication of SMPs. Ge Q, Sakhaei AH, Lee H, et al. [170] reported high resolution multimaterial architecture of SMP using 4D printing. This makes controlled shape memory properties achievable with designed constituents and compositions.

Combining geometrical shape-change with material shape-change is an emerging research direction, which is involved in studying mechanical instabilities of many kinds such as buckling, snapping, wrinkling, and creasing [171]. Thus, the bistability and multistability of SMAs and SMPs are achievable, and more advanced functions could be obtained for developing next generation biomedical devices for sensing and drug delivery. Applications such as these also pose the practical challenge of how to effectively scale down the system to the micro- and nanoscale. Last but not least, current SMAs and SMPs based devices still need external stimuli to trigger shape changes. Intelligent medical devices that have pre-programmed temporal shape evolution in absence of external stimuli or that can be triggered with dynamic material properties such as the presence of biomarkers point to future research directions [101].

6. Summary

SMAs and SMPs are the primary shape memory materials used in the biomedical field. They both demonstrate the capability of remembering multiple shapes and can change from one state to another under external stimulus. This review highlights key contributions in the past and recent studies on shape memory mechanisms and their biomedical applications. We discuss the mechanical biocompatibility of these materials under various deformation modes towards biomedical applications. Mechanical properties, such as elastic modulus, strength, fracture toughness, and fatigue need to be carefully evaluated prior to actual practice. Previous experimental studies have shown that the mechanical properties of shape memory materials are influenced by internal microstructures, such as grain size and cross link density, fracture toughness, fatigue, and environmental factors such as temperature and loading. Computational modeling has been used as a supplemental tool to assist in the design of shape memory materials and can reduce the complexity of experimental studies. Complex design of shape memory materials can be challenging with traditional fabrication methods, and thus the use of additive manufacturing methods is the future of making complex shape memory materials and biomedical devices.

Acknowledgement

Z.C. acknowledges the startup fund from the Thayer School of Engineering and the Branco Weiss—Society in Science fellowship (administered by ETH Zürich).

Conflict of interest

All authors declare no conflicts of interest in this paper.

References

1. Huang WM, Ding Z, Wang CC, et al. (2010) Shape memory materials. *Mater Today* 13: 54–61.
2. Ji F, Zhu Y, Hu J, et al. (2006) Smart polymer fibers with shape memory effect. *Smart Mater Struct* 15: 1547.
3. Petrini L, Migliavacca F (2011) Biomedical applications of shape memory alloys. *J Metall* 2011: 1–14.
4. Cho JW, Kim JW, Jung YC, et al. (2005) Electroactive shape-memory polyurethane composites incorporating carbon nanotubes. *Macromol Rapid Commun* 26: 412–416.
5. Lendlein A, Jiang H, Junger O, et al. (2005) Light-induced shape-memory polymers. *Nature* 434: 879–882.
6. Lendlein A, Schmidt AM, Schroeter M, et al. (2005) Shape-memory polymer networks from oligo (ϵ-caprolactone) dimethacrylates. *J Polym Sci, Part A: Polym Chem* 43: 1369–1381.
7. Tzou H, Lee HJ, Arnold S (2004) Smart materials, precision sensors/actuators, smart structures, and structronic systems. *Mech Adv Mater Struct* 11: 367–393.
8. Behl M, Lendlein A (2007) Shape-memory polymers. *Mater Today* 10: 20–28.
9. Wei Z, Sandstroröm R, Miyazaki S (1998) Shape-memory materials and hybrid composites for smart systems: Part I Shape-memory materials. *J Mater Sci* 33: 3743–3762.

10. El Feninat F, Laroche G, Fiset M, et al. (2002) Shape memory materials for biomedical applications. *Adv Eng Mater* 4: 91.
11. Hornbogen E (2006) Comparison of shape memory metals and polymers. *Adv Eng Mater* 8: 101–106.
12. Gunes IS, Jana SC (2008) Shape memory polymers and their nanocomposites: A review of science and technology of new multifunctional materials. *J Nanosci Nanotechnol* 8: 1616–1637.
13. Ma J, Karaman I, Noebe RD (2010) High temperature shape memory alloys. *Int Mater Rev* 55: 257–315.
14. Tsuchiya K (2011) Mechanisms and properties of shape memory effect and superelasticity in alloys and other materials: A practical guide, In: *Shape Memory and Superelastic Alloys*, Woodhead Publishing, 3–14.
15. Leng J, Lan X, Liu Y, et al. (2011) Shape-memory polymers and their composites: Stimulus methods and applications. *Prog Mater Sci* 56: 1077–1135.
16. Rousseau IA (2008) Challenges of shape memory polymers: A review of the progress toward overcoming SMP's limitations. *Polym Eng Sci* 48: 2075–2089.
17. Es-Souni M, Fischer-Brandies H (2005) Assessing the biocompatibility of NiTi shape memory alloys used for medical applications. *Anal Bioanal Chem* 381: 557–567.
18. Geetha M, Singh A, Asokamani R, et al. (2009) Ti based biomaterials, the ultimate choice for orthopaedic implants—a review. *Prog Mater Sci* 54: 397–425.
19. De Nardo L, Bertoldi S, Tanzi M, et al. (2011) Shape memory polymer cellular solid design for medical applications. *Smart Mater Struct* 20: 035004.
20. Robertson S, Pelton A, Ritchie R (2012) Mechanical fatigue and fracture of Nitinol. *Int Mater Rev* 57: 1–37.
21. Schroeder T, Wayman C (1977) The two-way shape memory effect and other "training" phenomena in Cu-Zn single crystals. *Scr Metall* 11: 225–230.
22. Perkins J, Hodgson D (1990) The two-way shape memory effect. *Eng Aspects Shape Mem Alloys* 1990: 195–206.
23. Huang W, Toh W (2000) Training two-way shape memory alloy by reheat treatment. *J Mater Sci Lett* 19: 1549–1550.
24. Otsuka K, Ren X (2005) Physical metallurgy of Ti—Ni-based shape memory alloys. *Prog Mater Sci* 50: 511–678.
25. Huang W (2002) On the selection of shape memory alloys for actuators. *Mater Des* 23: 11–19.
26. Huang WM, Song CL, Fu YQ, et al. (2013) Shaping tissue with shape memory materials. *Adv Drug Delivery Rev* 65: 515–535.
27. Carroll MC, Somsen C, Eggeler G (2004) Multiple-step martensitic transformations in Ni-rich NiTi shape memory alloys. *Scr Mater* 50: 187–192.
28. Zhou Y, Fan G, Zhang J, et al. (2006) Understanding of multi-stage R-phase transformation in aged Ni-rich Ti-Ni shape memory alloys. *Mater Sci Eng A* S438–440: 602–607.
29. Fujishima K, Nishida M, Morizono Y, et al. (2006) Effect of heat treatment atmosphere on the multistage martensitic transformation in aged Ni-rich Ti—Ni alloys. *Mater Sci Eng A* 438: 489–494.
30. Khalil-Allafi J, Dlouhy A, Eggeler G (2002) Ni4Ti3-precipitation during aging of NiTi shape memory alloys and its influence on martensitic phase transformations. *Acta Mater* 50: 4255–4274.

31. Wagner MFX, Dey SR, Gugel H, et al. (2010) Effect of low-temperature precipitation on the transformation characteristics of Ni-rich NiTi shape memory alloys during thermal cycling. *Intermetallics* 18: 1172–1179.
32. Kim JI, Liu Y, Miyazaki S (2004) Ageing-induced two-stage R-phase transformation in Ti—50.9at.%Ni. *Acta Mater* 52: 487–499.
33. Qin Q, Peng H, Fan Q, et al. (2018) Effect of second phase precipitation on martensitic transformation and hardness in highly Ni-rich NiTi alloys. *J Alloys Compd* 739: 873–881.
34. Luo J, Bobanga JO, Lewandowski JJ (2017) Microstructural heterogeneity and texture of as-received, vacuum arc-cast, extruded, and re-extruded NiTi shape memory alloy. *J Alloys Compd* 712: 494–509.
35. Luo J, Ye WJ, Ma XX, et al. (2018) The evolution and effects of second phase particles during hot extrusion and re-extrusion of a NiTi shape memory alloy. *J Alloys Compd* 735: 1145–1151.
36. Jani JM, Leary M, Subic A, et al. (2014) A review of shape memory alloy research, applications and opportunities. *Mater Des* 56: 1078–1113.
37. Maruyama T, Kubo H (2011) 12-Ferrous (Fe-based) shape memory alloys (SMAs): Properties, processing and applications, In: *Shape Memory and Superelastic Alloys*, Woodhead Publishing, 141–159.
38. Yamauchi K (2011) 3-Development and commercialization of titanium-nickel (Ti-Ni) and copper (Cu)-based shape memory alloys (SMAs), In: *Shape Memory and Superelastic Alloys*, Woodhead Publishing, 43–52.
39. Wadood A (2016) Brief overview on nitinol as biomaterial. *Adv Mater Sci Eng* 2016: 1–9.
40. Buehler WJ, Wang FE (1968) A summary of recent research on the nitinol alloys and their potential application in ocean engineering. *Ocean Eng* 1: 105–120.
41. Dikici B, Esen Z, Duygulu O, et al. (2015) Corrosion of metallic biomaterials, In: *Advances in Metallic Biomaterials*, Springer, 275–303.
42. Mantovani D (2000) Shape memory alloys: Properties and biomedical applications. *JOM* 52: 36–44.
43. Ryhänen J, Kallioinen M, Tuukkanen J, et al. (1998) In vivo biocompatibility evaluation of nickel-titanium shape memory metal alloy: Muscle and perineural tissue responses and encapsule membrane thickness. *J Biomed Mater Res* 41: 481–488.
44. Duerig T, Pelton A, Stöckel D (1999) An overview of nitinol medical applications. *Mater Sci Eng A* 273: 149–160.
45. Morgan N (2004) Medical shape memory alloy applications—the market and its products. *Mater Sci Eng A* 378: 16–23.
46. Dahlgren JM, Gelbart D (2009) System for mechanical adjustment of medical implants. Google Patents.
47. Pfeifer R, Müller CW, Hurschler C, et al. (2013) Adaptable orthopedic shape memory implants. *Procedia Cirp* 5: 253–258.
48. Maynard RS (1999) Distributed activator for a two-dimensional shape memory alloy. Google Patents.
49. Zider RB, Krumme JF (1988) Eyeglass frame including shape-memory elements. Google Patents.
50. Lim G, Park K, Sugihara M, et al. (1996) Future of active catheters. *Sens Actuators A* 56: 113–121.
51. Tung AT, Park BH, Liang DH, et al. (2008) Laser-machined shape memory alloy sensors for position feedback in active catheters. *Sens Actuators A* 147: 83–92.
52. Pelton A, Schroeder V, Mitchell M, et al. (2008) Fatigue and durability of Nitinol stents. *J Mech Behav Biomed Mater* 1: 153–164.
53. Dye D (2015) Shape memory alloys: Towards practical actuators. *Nat Mater* 14: 760–761.

54. Ogawa Y, Ando D, Sutou Y, et al. (2016) A lightweight shape-memory magnesium alloy. *Science* 353: 368.
55. Schone AC, Schulz B, Lendlein A (2016) Stimuli responsive and multifunctional polymers: progress in materials and applications. *Macromol Rapid Commun* 37: 1856–1859.
56. Cao Y, Xu S, Li L, et al. (2017) Physically cross-linked networks of POSS-capped poly(acrylate amide)s: Synthesis, morphologies, and shape memory behavior. *J Polym Sci, Part B: Polym Phys* 55: 587–600.
57. Momtaz M, Razavi-Nouri M, Barikani M (2014) Effect of block ratio and strain amplitude on thermal, structural, and shape memory properties of segmented polycaprolactone-based polyurethanes. *J Mater Sci* 49: 7575–7584.
58. Momtaz M, Barikani M, Razavi-Nouri M (2015) Effect of ionic group content on thermal and structural properties of polycaprolactone-based shape memory polyurethane ionomers. *Iran Polym J* 24: 505–513.
59. Saed MO, Torbati AH, Starr CA, et al. (2017) Thiol-acrylate main-chain liquid-crystalline elastomers with tunable thermomechanical properties and actuation strain. *J Polym Sci, Part B: Polym Phys* 55: 157–168.
60. Yang B, Huang WM, Li C, et al. (2006) Effects of moisture on the thermomechanical properties of a polyurethane shape memory polymer. *Polymer* 47: 1348–1356.
61. Gyarmati B, Mészár EZ, Kiss L, et al. (2015) Supermacroporous chemically cross-linked poly(aspartic acid) hydrogels. *Acta Biomater* 22: 32–38.
62. Guo W, Lu CH, Orbach R, et al. (2015) pH-stimulated DNA hydrogels exhibiting shape-memory properties. *Adv Mater* 27: 73–78.
63. Xie H, He MJ, Deng XY, et al. (2016) Design of poly(l-lactide)-poly(ethylene glycol) copolymer with light-induced shape-memory effect triggered by pendant anthracene groups. *ACS Appl Mater Interfaces* 8: 9431–9439.
64. Park J, Yoo JW, Seo HW, et al. (2017) Electrically controllable twisted-coiled artificial muscle actuators using surface-modified polyester fibers. *Smart Mater Struct* 26: 035048.
65. Zou H, Weder C, Simon YC (2015) Shape-Memory Polyurethane Nanocomposites with Single Layer or Bilayer Oleic Acid-Coated Fe3O4 Nanoparticles. *Macromol Mater Eng* 300: 885–892.
66. Voit W, Ware T, Gall K (2010) Radiation crosslinked shape-memory polymers. *Polymer* 51: 3551–3559.
67. Small Iv W, Wilson T, Benett W, et al. (2005) Laser-activated shape memory polymer intravascular thrombectomy device. *Opt Express* 13: 8204–8213.
68. Zhang F, Zhou T, Liu Y, et al. (2015) Microwave synthesis and actuation of shape memory polycaprolactone foams with high speed. *Sci Rep* 5: 11152.
69. Du H, Song Z, Wang J, et al. (2015) Microwave-induced shape-memory effect of silicon carbide/poly(vinyl alcohol) composite. *Sens Actuators A* 228: 1–8.
70. Fang Y, Ni Y, Leo SY, et al. (2015) Reconfigurable photonic crystals enabled by pressure-responsive shape-memory polymers. *Nat Commun* 6: 7416.
71. Fang Y, Ni Y, Choi B, et al. (2015) Chromogenic photonic crystals enabled by novel vapor-responsive shape-memory polymers. *Adv Mater* 27: 3696–3704.
72. Hu J, Zhu Y, Huang H, et al. (2012) Recent advances in shape-memory polymers: Structure, mechanism, functionality, modeling and applications. *Prog Polym Sci* 37: 1720–1763.
73. Liu C, Qin H, Mather P (2007) Review of progress in shape-memory polymers. *J Mater Chem* 17: 1543–1558.

74. Ahn Sk, Kasi RM (2011) Exploiting microphase-separated morphologies of side-chain liquid crystalline polymer networks for triple shape memory properties. *Adv Funct Mater* 21: 4543–4549.
75. Luo X, Mather PT (2010) Triple-shape polymeric composites (TSPCs). *Adv Funct Mater* 20: 2649–2656.
76. Wang L, Yang X, Chen H, et al. (2013) Design of triple-shape memory polyurethane with photo-cross-linking of cinnamon groups. *ACS Appl Mater Interfaces* 5: 10520–10528.
77. Wang L, Yang X, Chen H, et al. (2013) Multi-stimuli sensitive shape memory poly(vinyl alcohol)-graft-polyurethane. *Polym Chem* 4: 4461–4468.
78. Wang L, Wang W, Di S, et al. (2014) Silver-coordination polymer network combining antibacterial action and shape memory capabilities. *RSC Adv* 4: 32276–32282.
79. Behl M, Kratz K, Zotzmann J, et al. (2013) Reversible bidirectional shape-memory polymers. *Adv Mater* 25: 4466–4469.
80. Zhou J, Turner SA, Brosnan SM, et al. (2014) Shapeshifting: Reversible shape memory in semicrystalline elastomers. *Macromolecules* 47: 1768–1776.
81. Miaudet P, Derré A, Maugey M, et al. (2007) Shape and temperature memory of nanocomposites with broadened glass transition. *Science* 318: 1294–1296.
82. Behl M, Kratz K, Noechel U, et al. (2013) Temperature-memory polymer actuators. *Proc Natl Acad Sci* 110: 12555–12559.
83. Wang L, Di S, Wang W, et al. (2014) Tunable temperature memory effect of photo-cross-linked star PCL—PEG networks. *Macromolecules* 47: 1828–1836.
84. Hu J (2007) Shape memory textiles, In: *Shape Memory Polymers and Textiles*, Woodhead Publishing, 305–337.
85. Yanju L, Haiyang D, Liwu L, et al. (2014) Shape memory polymers and their composites in aerospace applications: A review. *Smart Mater Struct* 23: 023001.
86. Baudis S, Behl M, Lendlein A (2014) Smart polymers for biomedical applications. *Macromol Chem Phys* 215: 2399–2402.
87. Wache HM, Tartakowska DJ, Hentrich A, et al. (2003) Development of a polymer stent with shape memory effect as a drug delivery system. *J Mater Sci Mater Med* 14: 109–112.
88. Small W, Buckley PR, Wilson TS, et al. (2007) Shape memory polymer stent with expandable foam: A new concept for endovascular embolization of fusiform aneurysms. *IEEE Trans Biomed Eng* 54: 1157–1160.
89. Zheng Y, Li Y, Hu X, et al. (2017) Biocompatible shape memory blend for self-expandable stents with potential biomedical applications. *ACS Appl Mater Interfaces* 9: 13988.
90. Kularatne RS, Kim H, Boothby JM, et al. (2017) Liquid crystal elastomer actuators: Synthesis, alignment, and applications. *J Polym Sci, Part B: Polym Phys* 55: 395–411.
91. Zhang Y, Gao H, Wang H, et al. (2018) Radiopaque highly stiff and tough shape memory hydrogel microcoils for permanent embolization of arteries. *Adv Funct Mater* 28: 1705962.
92. Hager MD, Bode S, Weber C, et al. (2015) Shape memory polymers: Past, present and future developments. *Prog Polym Sci* 49: 3–33.
93. Kratz K, Voigt U, Lendlein A (2012) Temperature-memory effect of copolyesterurethanes and their application potential in minimally invasive medical technologies. *Adv Funct Mater* 22: 3057–3065.
94. Serrano MC, Ameer GA (2012) Recent insights into the biomedical applications of shape-memory polymers. *Macromol Biosci* 12: 1156–1171.

95. Small W, Singhal P, Wilson TS, et al. (2010) Biomedical applications of thermally activated shape memory polymers. *J Mater Chem* 20: 3356–3366.
96. Lendlein A, Langer R (2002) Biodegradable, elastic shape-memory polymers for potential biomedical applications. *Science* 296: 1673–1676.
97. Wischke C, Neffe AT, Steuer S, et al. (2009) Evaluation of a degradable shape-memory polymer network as matrix for controlled drug release. *J Controlled Release* 138: 243–250.
98. Balk M, Behl M, Wischke C, et al. (2016) Recent advances in degradable lactide-based shape-memory polymers. *Adv Drug Delivery Rev* 107: 136–152.
99. Yu K, Ritchie A, Mao Y, et al. (2015) Controlled sequential shape changing components by 3D printing of shape memory polymer multimaterials. *Procedia Iutam* 12: 193–203.
100. Hardy JG, Palma M, Wind SJ, et al. (2016) Responsive biomaterials: Advances in materials based on shape-memory polymers. *Adv Mater* 28: 5717–5724.
101. Chan BQY, Low ZWK, Heng SJW, et al. (2016) Recent advances in shape memory soft materials for biomedical applications. *ACS Appl Mater Interfaces* 8: 10070–10087.
102. Mazza E, Ehret AE (2015) Mechanical biocompatibility of highly deformable biomedical materials. *J Mech Behav Biomed Mater* 48: 100–124.
103. Niinomi M, Nakai M, Hieda J (2012) Development of new metallic alloys for biomedical applications. *Acta Biomater* 8: 3888–3903.
104. Niinomi M (2010) Tend and present state of titanium alloys with body centered structure for biomedical applications. *Bull Iron Steel Inst Jpn* 15: 661–670.
105. Tane M, Akita S, Nakano T, et al. (2008) Peculiar elastic behavior of Ti-Nb-Ta-Zr single crystals. *Acta Mater* 56: 2856–2863.
106. Sadrnezhaad SK, Hosseini SA (2009) Fabrication of porous NiTi-shape memory alloy objects by partially hydrided titanium powder for biomedical applications. *Mater Des* 30: 4483–4487.
107. Xiong J, Li Y, Wang X, et al. (2008) Titanium-nickel shape memory alloy foams for bone tissue engineering. *J Mech Behav Biomed Mater* 1: 269–273.
108. Oh IH, Nomura N, Hanada S (2002) Microstructures and mechanical properties of porous titanium compacts prepared by powder sintering. *Mater Trans* 43: 443–446.
109. Wang M, Jiang M, Liao G, et al. (2012) Martensitic transformation involved mechanical behaviors and wide hysteresis of NiTiNb shape memory alloys. *Prog Nat Sci Mater Int* 22: 130–138.
110. Chen J, Wang G, Sun W (2005) Investigation on the fracture behavior of shape memory alloy NiTi. *Metall Mater Trans A* 36: 941–955.
111. Kim HY, Hashimoto S, Kim JI, et al. (2004) Mechanical properties and shape memory behavior of Ti-Nb alloys. *Mater Trans* 45: 2443–2448.
112. Miyazaki S, Kim H, Hosoda H (2006) Development and characterization of Ni-free Ti-base shape memory and superelastic alloys. *Mater Sci Eng A* 438: 18–24.
113. Niinomi M (2003) Recent research and development in titanium alloys for biomedical applications and healthcare goods. *Sci Technol Adv Mater* 4: 445–454.
114. Mckelvey A, Ritchie R (2001) Fatigue-crack growth behavior in the superelastic and shape-memory alloy nitinol. *Metall Mater Trans A* 32: 731–743.
115. Robertson S, Mehta A, Pelton A, et al. (2007) Evolution of crack-tip transformation zones in superelastic nitinol subjected to in situ fatigue: A fracture mechanics and synchrotron X-ray microdiffraction analysis. *Acta Mater* 55: 6198–6207.

116. Figueiredo AM, Modenesi P, Buono V (2009) Low-cycle fatigue life of superelastic NiTi wires. *Int J Fatigue* 31: 751–758.
117. Yu XJ, Kumar KS (2012) Uniaxial, load-controlled cyclic deformation of recrystallized molybdenum sheet. *Mater Sci Eng A* 540: 187–197.
118. Yu XJ, Kumar KS (2016) Cyclic tensile response of Mo-27 at% Re and Mo-0.3 at% Si solid solution alloys. *Mater Sci Eng A* 676: 312–323.
119. Kim Y (2002) Fatigue properties of the Ti-Ni base shape memory alloy wire. *Mater Trans* 43: 1703–1706.
120. Pappas P, Bollas D, Parthenios J, et al. (2007) Transformation fatigue and stress relaxation of shape memory alloy wires. *Smart Mater Struct* 16: 2560.
121. Barrabés M, Sevilla P, Planell JA, et al. (2008) Mechanical properties of nickel—titanium foams for reconstructive orthopaedics. *Mater Sci Eng C* 28: 23–27.
122. Nayan N, Roy D, Buravalla V, et al. (2008) Unnotched fatigue behavior of an austenitic Ni—Ti shape memory alloy. *Mater Sci Eng A* 497: 333–340.
123. Kang G, Song D (2015) Review on structural fatigue of NiTi shape memory alloys: Pure mechanical and thermo-mechanical ones. *Theor Appl Mech Lett* 5: 245–254.
124. Zhang X, Liu H, Yuan B, et al. (2008) Superelasticity decay of porous NiTi shape memory alloys under cyclic strain-controlled fatigue conditions. *Mater Sci Eng A* 481: 170–173.
125. Fulcher J, Lu Y, Tandon G, et al. (2010) Thermomechanical characterization of shape memory polymers using high temperature nanoindentation. *Polym Test* 29: 544–552.
126. Schmidt C, Sarwaruddin Chowdhury AM, Neuking K, et al. (2011) Thermo-mechanical behaviour of shape memory polymers, e.g., Tecoflex® by 1WE method: SEM and IR analysis. *J Polym Res* 18: 1807–1812.
127. Di Prima M, Gall K, Mcdowell D, et al. (2010) Cyclic compression behavior of epoxy shape memory polymer foam. *Mech Mater* 42: 405–416.
128. Ahmad M, Xu B, Purnawali H, et al. (2012) High performance shape memory polyurethane synthesized with high molecular weight polyol as the soft segment. *Appl Sci* 2: 535.
129. Kang SM, Lee SJ, Kim BK (2012) Shape memory polyurethane foams. *eXPRESS Polym Lett* 6: 63–69.
130. Zhang H, Wang H, Zhong W, et al. (2009) A novel type of shape memory polymer blend and the shape memory mechanism. *Polymer* 50: 1596–1601.
131. Guo J, Wang Z, Tong L, et al. (2015) Shape memory and thermo-mechanical properties of shape memory polymer/carbon fiber composites. *Composites Part A* 76: 162–171.
132. Ni QQ, Zhang CS, Fu Y, et al. (2007) Shape memory effect and mechanical properties of carbon nanotube/shape memory polymer nanocomposites. *Compos Struct* 81: 176–184.
133. Mohr R, Kratz K, Weigel T, et al. (2006) Initiation of shape-memory effect by inductive heating of magnetic nanoparticles in thermoplastic polymers. *Proc Natl Acad Sci U S A* 103: 3540–3545.
134. Xu B, Fu YQ, Ahmad M, et al. (2010) Thermo-mechanical properties of polystyrene-based shape memory nanocomposites. *J Mater Chem* 20: 3442–3448.
135. Zheng X, Zhou S, Li X, et al. (2006) Shape memory properties of poly(d,l-lactide)/hydroxyapatite composites. *Biomaterials* 27: 4288–4295.
136. Wei H, Zhang F, Zhang D, et al. (2015) Shape-memory behaviors of electrospun chitosan/poly(ethylene oxide) composite nanofibrous membranes. *J Appl Polym Sci* 132: n/a.

137. Cisse C, Zaki W, Zineb TB (2016) A review of modeling techniques for advanced effects in shape memory alloy behavior. *Smart Mater Struct* 25: 103001.
138. Zhang L, Du H, Liu L, et al. (2014) Analysis and design of smart mandrels using shape memory polymers. *Composites Part B* 59: 230–237.
139. Mirzaeifar R, DesRoches R, Yavari A (2011) Analysis of the rate-dependent coupled thermo-mechanical response of shape memory alloy bars and wires in tension. *Continuum Mech Thermodyn* 23: 363–385.
140. Uehara T, Asai C, Ohno N (2009) Molecular dynamics simulation of shape memory behaviour using a multi-grain model. *Modell Simul Mater Sci Eng* 17: 035011.
141. Pun GP, Mishin Y (2010) Molecular dynamics simulation of the martensitic phase transformation in NiAl alloys. *J Phys Condens Matter* 22: 395403.
142. Zhong Y, Zhu T (2014) Phase-field modeling of martensitic microstructure in NiTi shape memory alloys. *Acta Mater* 75: 337–347.
143. Nguyen TD (2013) Modeling shape-memory behavior of polymers. *Polym Rev* 53: 130–152.
144. Leclercq S, Lexcellent C (1996) A general macroscopic description of the thermomechanical behavior of shape memory alloys. *J Mech Phys Solids* 44: 953–980.
145. Falk F (1980) Model free energy, mechanics, and thermodynamics of shape memory alloys. *Acta Metall* 28: 1773–1780.
146. Paiva A, Savi MA (2006) An overview of constitutive models for shape memory alloys. *Math Probl Eng* 2006: 39–62.
147. Tanaka K, Nagaki S (1982) A thermomechanical description of materials with internal variables in the process of phase transitions. *Ing Arch* 51: 287–299.
148. Liang C, Rogers CA (1990) One-dimensional thermomechanical constitutive relations for shape memory materials. *J Intell Mater Syst Struct* 1: 207–234.
149. Brinson LC (1993) One-dimensional constitutive behavior of shape memory alloys: Thermomechanical derivation with non-constant material functions and redefined martensite internal variable. *J Intell Mater Syst Struct* 4: 229–242.
150. Panico M, Brinson L (2007) A three-dimensional phenomenological model for martensite reorientation in shape memory alloys. *J Mech Phys Solids* 55: 2491–2511.
151. Bouvet C, Calloch S, Taillard K, et al. (2004) Experimental determination of initial surface of phase transformation of SMA. *J Phys IV Fr* 115: 29–36.
152. Arghavani J, Auricchio F, Naghdabadi R, et al. (2010) A 3-D phenomenological constitutive model for shape memory alloys under multiaxial loadings. *Int J Plast* 26: 976–991.
153. Moumni Z, Zaki W, Maitournam H (2009) Cyclic behavior and energy approach to the fatigue of shape memory alloys. *J Mech Mater Struct* 4: 395–411.
154. Zhang Q, Yang QS (2012) Recent advance on constitutive models of thermal-sensitive shape memory polymers. *J Appl Polym Sci* 123: 1502–1508.
155. Srivastava V, Chester SA, Anand L (2010) Thermally actuated shape-memory polymers: Experiments, theory, and numerical simulations. *J Mech Phys Solids* 58: 1100–1124.
156. Liu Y, Gall K, Dunn ML, et al. (2006) Thermomechanics of shape memory polymers: Uniaxial experiments and constitutive modeling. *Int J Plast* 22: 279–313.
157. Diani J, Liu Y, Gall K (2006) Finite strain 3D thermoviscoelastic constitutive model for shape memory polymers. *Polym Eng Sci* 46: 486–492.

158. Li G, Xu W (2011) Thermomechanical behavior of thermoset shape memory polymer programmed by cold-compression: Testing and constitutive modeling. *J Mech Phys Solids* 59: 1231–1250.
159. Baghani M, Naghdabadi R, Arghavani J, et al. (2012) A thermodynamically-consistent 3D constitutive model for shape memory polymers. *Int J Plast* 35: 13–30.
160. Wever D, Veldhuizen A, Sanders M, et al. (1997) Cytotoxic, allergic and genotoxic activity of a nickel-titanium alloy. *Biomaterials* 18: 1115–1120.
161. Shayan M, Chun Y (2015) An overview of thin film nitinol endovascular devices. *Acta Biomater* 21: 20–34.
162. Cui ZD, Man HC, Yang XJ (2005) The corrosion and nickel release behavior of laser surface-melted NiTi shape memory alloy in Hanks' solution. *Surf Coat Technol* 192: 347–353.
163. Cheng Y, Cai W, Li H, et al. (2004) Surface characteristics and corrosion resistance properties of TiNi shape memory alloy coated with Ta. *Surf Coat Technol* 186: 346–352.
164. Firstov G, Vitchev R, Kumar H, et al. (2002) Surface oxidation of NiTi shape memory alloy. *Biomaterials* 23: 4863–4871.
165. Poon R, Yeung K, Liu X, et al. (2005) Carbon plasma immersion ion implantation of nickel-titanium shape memory alloys. *Biomaterials* 26: 2265–2272.
166. Chen M, Yang X, Liu Y, et al. (2003) Study on the formation of an apatite layer on NiTi shape memory alloy using a chemical treatment method. *Surf Coat Technol* 173: 229–234.
167. Chu C, Hu T, Wu S, et al. (2007) Surface structure and properties of biomedical NiTi shape memory alloy after Fenton's oxidation. *Acta Biomater* 3: 795–806.
168. Hu T, Wen C, Sun G, et al. (2010) Wear resistance of NiTi alloy after surface mechanical attrition treatment. *Surf Coat Technol* 205: 506–510.
169. Walker J, Andani MT, Haberland C, et al. (2014) Additive manufacturing of Nitinol shape memory alloys to overcome challenges in conventional Nitinol fabrication. Proceedings of the ASME 2014 IMECE, V02AT02A037.
170. Ge Q, Sakhaei AH, Lee H, et al. (2016) Multimaterial 4D printing with tailorable shape memory polymers. *Sci Rep* 6: 31110.
171. Hu N, Burgueño R (2015) Buckling-induced smart applications: Recent advances and trends. *Smart Mater Struct* 24.

AIMS Press